THE ASTROPHYSICAL JOURNAL, 626:1091–1095, 2005 June 20

ON THE AVAILABILITY OF SUFFICIENT TWIST IN SOLAR ACTIVE REGIONS TO TRIGGER THE KINK INSTABILITY

K. D. LEKA
Colorado Research Associates Division, NorthWest Research Associates, Inc., 3380 Mitchell Lane,
Boulder, CO 80301; leka@cora.nwra.com

AND

Y. FAN AND G. BARNES[1]
High Altitude Observatory, National Center for Atmospheric Research, P.O. Box 3000, Boulder, CO 80307;
yfan@hao.ucar.edu, graham@cora.nwra.com
Received 2004 November 30; accepted 2005 March 8

ABSTRACT

The question of whether there is sufficient magnetic twist in solar active regions for the onset of the kink instability is examined using a “blind test” of analysis methods commonly used to interpret observational data. “Photospheric magnetograms” are constructed from a recently developed numerical simulation of a kink-unstable emerging flux rope with nearly constant (negative) wind. The calculation of the best-fit linear force-free parameter $\alpha_{\rm best}$ is applied, with the goal of recovering the model input helicity. It is shown that for this simple magnetic structure, three effects combine to produce an underestimation of the known helicity: (1) the influence of horizontal fields with lower local α values within the flux rope; (2) an assumed simple relation between $\alpha_{\rm best}$ and the winding rate q does not apply to nonaxis fields in a flux rope that is not thin; and (3) the difficulty in interpreting the force-free twist parameter measured for a field that is *forced*. A different method to evaluate the magnetic twist in active region flux ropes is presented, which is based on evaluating the peak α value at the flux rope axis. When applied to data from the numerical simulation, the twist component of the magnetic helicity is essentially recovered. Both the $\alpha_{\rm best}$ and the new $\alpha_{\rm peak}$ methods are then applied to observational photospheric vector magnetic field data of NOAA AR 7201. The $\alpha_{\rm best}$ approach is then confounded further in NOAA AR 7201 by a distribution of α that contains both signs, as is generally observed in active regions. The result from the proposed $\alpha_{\rm peak}$ approach suggests that a larger magnetic twist is present in this active region’s δ-spot than would have been inferred from $\alpha_{\rm best}$, by at least a factor of 3. It is argued that the magnetic fields in localized active region flux ropes may indeed carry greater than 2π winds, and thus the kink instability is a possible trigger mechanism for solar flares and coronal mass ejections.

Subject headings: Sun: activity — Sun: coronal mass ejections (CMEs) — Sun: magnetic fields — Sun: photosphere — sunspots

Online material: color figures

1. INTRODUCTION

While it is not yet known what process triggers solar energetic events, certain aspects of the magnetic field, as observed at the photospheric boundary, do appear to play a role. Numerous efforts have been undertaken to establish the statistical relation of the photospheric magnetic field to coronal mass ejections (CMEs; Falconer et al. 2002; Canfield et al. 1999) and solar flares (Leka & Barnes 2003), based on the hypothesis that measures derived from the photospheric magnetic field bear a direct physical relationship to the magnetic state of the corona. Establishing a statistical correlation is only the start and does not necessarily provide causality; the goal is to understand the requirements of the solar magnetic atmosphere to produce an eruption: what, if any, thresholds must be crossed and what the trigger mechanism(s) is(are).

The kink instability is the process whereby magnetic twist (winding of magnetic field lines around an axis) in a contained flux system is abruptly converted to magnetic writhe (the winding or deforming of the axis itself). The exact amount of twist T required to trigger a kink instability depends on numerous factors, including the loop geometry and neighboring/overlying fields, but is generally agreed to be at least one full wind (see discussions in Hood & Priest 1979; Priest 1987; Lionello et al. 1998; Baty et al. 1998; Baty 2001; Török et al. 2004; Fan & Gibson 2003, 2004). Recently, Leamon et al. (2003) tested the hypothesis that “twisted coronal loops are unstable to the MHD kink mode only if their total twist exceeds a critical value . . . not less than $T_c \approx 2\pi$”; a further hypothesis was introduced, in which the twist of interest was that associated with the “nonlocal” large scale or average for the active region. This observational study of active regions associated with eruptive events quantified the magnetic twist using the “best-fit” linear force-free magnetic twist parameter $\alpha_{\rm best}$ (Pevtsov et al. 1995; “$\alpha_{\rm ff}$” in Leka & Skumanich 1999), derived for the whole active region from photospheric magnetograms, assuming that it related to the winding rate q by a simple factor of 2. Coupled with a simple (and reasonable) model of the associated coronal magnetic loop length l as a semicircle between the two magnetic footpoints separated by distance d, the total twist was computed by Leamon et al. (2003) as

$$T = lq = \frac{\pi d}{2} \frac{\alpha_{\rm best}}{2}. \tag{1}$$

[1] Also at CoRA Division, NWRA, Inc.

The total twist inferred for most active regions in their sample barely achieved $T = 1.5$, corresponding to field lines winding a quarter turn about the axis (hereafter we use $T/2\pi$; i.e., in this case $T/2\pi = 0.25$). Such a small inferred total twist for a sample of 25 CME-producing active regions lead the authors to conclude that the results were "inconsistent with the kink instability as the cause of solar eruptions."

Here we demonstrate that, as acknowledged in Leamon et al. (2003), there may be ample twist available for active region coronal magnetic fields to undergo kink instability, albeit on smaller, localized scales. Using data from a numerical simulation, an analytic model, and the observed photospheric vector magnetic field, we examine the assumptions surrounding the calculations using α_{best} and the relation between the force-free twist parameter α and the twist component of the magnetic helicity. It is shown in §§ 2 and 3 that relying on α_{best} and the thin flux tube assumption leads to an underestimation of the twist, even when applied to a constant-wind flux rope structure. We propose in § 4 a modified method, which is shown to better recover the twist component of the magnetic helicity in the simulation data. In § 5, we demonstrate and discuss the differences between the α_{best} and new α_{peak} techniques in application to observational data of an active region that included a δ-spot.

2. TESTING α_{best} ON DATA FROM NUMERICAL SIMULATION

Can boundary magnetic field data provide sufficient information to interpret the state of the region above it? That is, can the photospheric vector magnetic field be used to characterize whether there is sufficient twist for the coronal field to become kink unstable?

To address this, we first turn to data from numerical simulations. Recently, an MHD model of a helicity-carrying magnetic flux system emerging into an overlying potential magnetic arcade was developed by Fan & Gibson (2003, 2004). During its evolution, the emerging flux rope becomes unstable to kinking and quickly rises, interacting with the overlying arcade in the process. Thus, these simulation data provide a known quantity to test; would this "active region" be suspected to become kink unstable were it observed on the Sun?

We focus first on a "snapshot" at time step 45, when the flux rope is almost completely emerged but the kinking has not yet manifested (see Fig. 2 of Fan & Gibson 2004). The known properties of the simulated coronal field at this time are as follows (see Table 1): the field lines in the emerged flux rope have a nearly constant winding rate, and wind an average 1.5 times between line-tied ends (i.e., $T/2\pi = 1.5$). The distance d between the axis "legs" at the boundary is $0.72L$, and the axial field line follows an approximately semicircular path of length $1.11L$. (L is the length scale for the model, effectively the box length in the $\hat{y}$-direction; it will be used herein when referring to the simulation data.)

Note that the above value of total twist of $T/2\pi = 1.5$ is obtained from the H/ϕ^2 computed in Fan & Gibson (2004) at time step 45. In computing the relative helicity H using equations (12)–(15) in Fan & Gibson (2004), the B field of the flux rope was isolated in the domain, and the arcade field was excluded (hence ϕ instead of total flux Φ) so that the computed H only contains the tube's self-helicity, and H/ϕ^2 corresponds to the total twist in the emerged tube.

We create a "photospheric vector magnetogram" (see Fig. 1) from a cross-section of the simulation data just slightly above the lower boundary, at a height $z = 0.006L$. The footpoints of the flux tube determined by the locations of maximum vertical field are separated by $0.69L$, slightly shorter than the known axis separation. The implied semicircular loop length is thus $1.09L$, slightly shorter than the axial field line.

TABLE 1
Measures of Twist in the Fan & Gibson (2004) Model

Object	α (L^{-1})	d (L)	l (L)	$T/2\pi$
Time Step 45				
Model field	. . .	0.72	1.11	1.5
α_{best} Method				
$z = 0.006L$:				
Active region	-7.5 ± 1.3	0.694	1.09[a]	0.65 ± 0.11
Flux rope	-9.1 ± 1.0	. . .	. . .	0.80 ± 0.09
$z = 0.031L$:				
Active region	-7.2 ± 0.7	0.695	1.09[a]	0.62 ± 0.06
Flux rope	-9.9 ± 1.0	. . .	. . .	0.86 ± 0.09
α_{peak} Method				
Flux rope	-17.5	0.72	1.13[a]	1.57
Time Step 30				
Model field	. . .	0.45	0.48	0.77
α_{peak} Method				
Flux rope	-18.2	0.46	0.72[a]	1.04
	-18.2	. . .	0.48	0.69

[a] Assuming $l = \pi d/2$, i.e., a semicircle.

The parameter α_{best} is that value of α that gives the best agreement between a linear force-free field computed from the observed B_z and the observed horizontal field. Thus α_{best} acts as a spatial average weighted by the horizontal field. From the photospheric vector magnetogram derived from the simulation at time step 45, $\alpha_{\mathrm{best}} = -7.5 \pm 1.3\ L^{-1}$. Paired with the semicircle loop length and the uncertainties in α_{best}, equation (1) gives the inferred wind number $T/2\pi = 0.65$ (Table 1).

As with solar active regions, there is a mix of twisted and untwisted magnetic field in the simulation, the latter being composed of the potential-field arcade, which overlies the emerging flux rope. Isolating the flux rope (see Fig. 1, *boxed area*) results in the slightly larger $\alpha_{\mathrm{best}} = -9.1 \pm 1.0\ L^{-1}$. In combination with the same loop length, $T/2\pi = 0.8$, which is slightly larger but still below the "minimum critical" $1 \times 2\pi$ discussed in Leamon et al. (2003). This resulting $T/2\pi$ wind number is also well below the known model field discussed above (and summarized in Table 1).

3. IMPLICATIONS FOR MEASURING MAGNETIC TWIST

Why do we fail to reproduce the known inputs in this blind test? We point out three reasons.

The first concerns the assumption that α_{best}, as a single weighted average (Leka & Skumanich 1999), adequately describes a system in which a significant variation exists. Due to the strong influence of horizontal fields on the calculation of α_{best}, the result is dependent on an interplay between the distribution of B_z, B_h, and J_z magnitudes.

Consider α_z, described by the distribution of J_z/B_z, rather than α_{best} (see Fig. 2). Keeping in mind that the flux rope has nearly constant wind, and thus the local $\alpha(x,y) \propto (J_z/B_z)(x,y)$

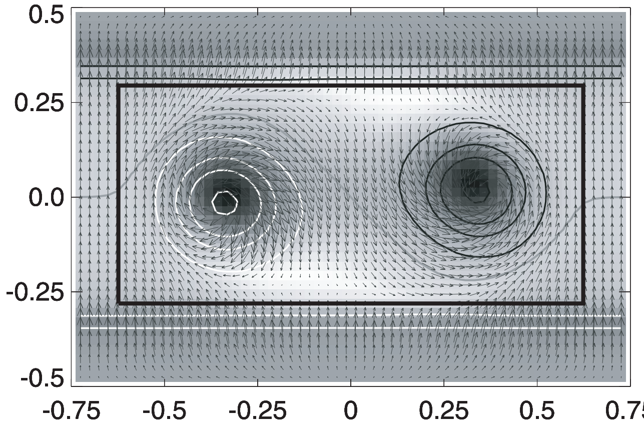

FIG. 1.—Vector magnetic field at $z = 0.006L$ from the numerical simulation of Fan & Gibson (2004), at time step 45. Underlying "continuum image" is a reverse-color image of B^2; positive(negative) vertical magnetic flux is indicated by white(black) solid lines at 100, 500, 1000, and 2000 G, and the magnetic polarity inversion lines are also indicated by the gray contour. Horizontal magnetic field is plotted at every fourth pixel. Tick marks are in units of L. The black box outlines the subarea used when the flux rope is isolated. [*See the electronic edition of the Journal for a color version of this figure.*]

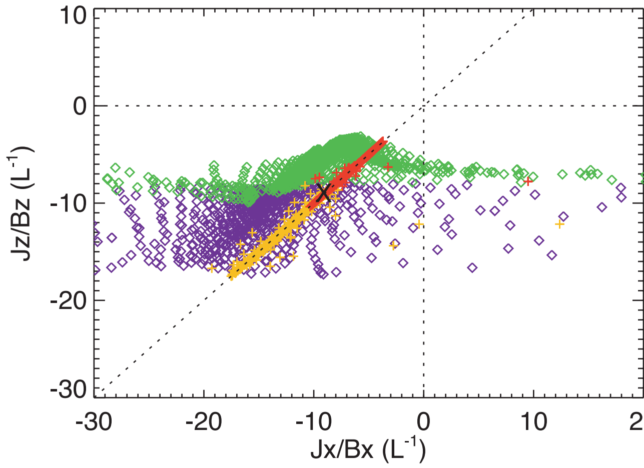

FIG. 2.—Scatter plot of $\alpha_x = J_x/B_x$ vs. $\alpha_z = J_z/B_z$ for heights $z = 0.006L$ (*purple and green diamonds, respectively*) and $z = 0.031L$ (*red and yellow plus signs, respectively*). The points for near-axis more vertical fields are those with generally larger $|\alpha_z|$ (*purple and yellow symbols*), compared to those for fields more inclined toward the horizontal and within the flux tube but away from the axis (*green and red symbols*). The $\alpha_{\rm best} = -9.1L^{-1}$ derived for the flux rope is indicated by a large black "X." Of note: (1) the influence of the inclined-field regions on $\alpha_{\rm best}$ is clear as the distinct difference between α_z for the more vertical and more inclined regions (purple vs. green for $z = 0.006L$; yellow vs. red for $z = 0.031L$); (2) α_x has little relation to α_z at $z = 0.006L$ (*diamonds*), indicating that the layer is not force free. At $z = 0.031L$, however (*plus signs*), there is a direct relation between the directed current/flux ratios, implying that the layer is force free and that the parameter α can be related to the twist present.

stays predominantly negative, we see that where the fields are strong and primarily vertical (close to the axis), $\langle \alpha_z(x, y)\rangle = \langle J_z/B_z(x, y)\rangle = -13.3 \pm 1.9\ L^{-1}$, whereas in regions of more inclined field away from the tube axis $\langle \alpha_z \rangle = -5.8 \pm 3.0\ L^{-1}$. That is, $\alpha_{\rm best}$ represents the average α away from the axis.

The presence of the potential $\alpha_z = 0$ arcade and the additional dilution it brings to $\alpha_{\rm best}$ explains the difference between $\alpha_{\rm best}$ of the isolated flux rope and the full "active region." As shown in Pevtsov et al. (1994), Leka & Skumanich (1999), and Leka (1999), active regions can display a wide range of local $\alpha(x, y)$, which generally fall on both sides of zero. Measures such as $\alpha_{\rm best}$ thus result in robust averages of nearly zero (see also Fig. 3 of Leka & Skumanich 1999 and Fig. 9 of Leka 1999; and § 4). For this blind test, however, the averaging effect of opposite-sign twist is *not* a strong factor in the $\alpha_{\rm best}$ results; the variation of $\alpha(x, y)$ is primarily a function of the distance from the axis.

Why does $\alpha_{\rm best}$ not recover the twist component of the helicity even for a constant-wind construct? This brings us to the second reason, for which an analytical example is illustrative. Consider a simple Gold-Hoyle–type force-free flux tube (Gold & Hoyle 1960) with

$$B_z = \frac{B_0}{(1 + q^2 r^2)}, \quad B_\theta = qrB_z, \tag{2}$$

which is nonlinear force free and uniformly twisted (q, the twist per unit length, is constant with radius r; see, for example, Priest 1987, § 7.4). All field lines wind about the axis by the same amount over a fixed distance along the tube. Evaluating $\alpha_z = J_z/B_z$ directly, $\alpha_z(r) = 2q/(1 + q^2 r^2)$, which peaks for the axial field line at $r = 0$ but decreases with increasing r. If the flux rope is thin in the sense that the radius of the tube is small compared to all other relevant length scales, in this case $qr \ll 1$, then $\alpha_z(r)$ is essentially constant, and $\alpha_{\rm best} \simeq \alpha_z(r) \simeq 2q$. If, however, the flux rope is *not* thin, then *at the axis* $\alpha_z(r = 0) = 2q$, but over the rest of the tube $\alpha_z(r)$ varies, and taking $2q = \alpha_{\rm best} = \langle \alpha_z \rangle$ underestimates q.

In the context of the simulation data, the model flux rope is not thin, and thus invoking the thin flux tube approximation in order to measure $T/2\pi$ using the $2q = \alpha_{\rm best}$ assumption (eq. [1]) underestimates the total twist. In the case of Leamon et al. (2003, 2004), the $2q = \alpha_{\rm best}$ assumption was invoked for entire active regions, and the twist—even the large-scale twist—was underestimated.

The third reason we fail to reproduce the inputs is that α_z in the photosphere, derived by whatever means, may bear little resemblance to the true magnetic twist due to the fact that the field is not force free, i.e., $\boldsymbol{J} \times \boldsymbol{B} \neq 0$. This is distinctly the case at $z = 0.006L$ near the line-tied lower boundary in the simulation (see Fig. 2), where $\alpha_z = J_z/B_z$ does not well represent the situation for $\alpha_x = J_x/B_x$ (similarly for $\hat{y}$). Thus, α computed in a forced layer cannot represent a force-free twist parameter.

Using the simulation data, a "chromospheric vector magnetogram" is created at $z = 0.031L$, where now indeed $\boldsymbol{J} \parallel \boldsymbol{B}$ (Fig. 2). The results for $\alpha_{\rm best}$ are not significantly different (see Table 1). Thus, even though the field is force free, $\alpha(x, y)$ *still* has a wide variation, and $\alpha_{\rm best}$ *still* acts as an average, but now there is a unique relation between α_x and α_z such that the state of the field might be interpreted from an observed (single-height) vector field boundary.

4. RECOVERING THE TWIST: THE $\alpha_{\rm peak}$ APPROACH

The twist component of the total magnetic helicity in a uniformly wound flux tube is $\mathrm{Tw} = (ql/2\pi)\Phi^2$, with q and l defined as above and Φ the magnetic flux (Moffatt & Ricca 1992; Longcope & Klapper 1997; Longcope et al. 1998). Assuming constant winding, it was demonstrated above that q can be recovered using α derived from a boundary vector magnetic field *on the axis* of the tube. That is, if there is no writhe and q is constant, the axis should correspond to the region of largest α, and using that value rather than an average α should recover $T = ql$ more readily.

Using the "chromospheric magnetogram" at $z = 0.031L$, the peak $\alpha_z = J_z/B_z$ near the axis is $-17.5L^{-1}$ and $l = 1.13L^{-1}$, giving $\mathrm{Tw}/\Phi^2 = T/2\pi = 1.6$ for the twist component of the magnetic helicity. This result almost exactly agrees with the total

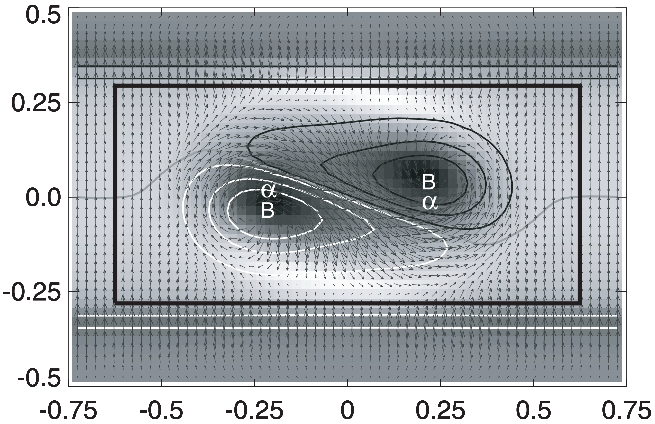

FIG. 3.—Same as Fig. 1 but for time step 30. The peak B_z locations are marked with "B," and the locations of peak α are marked with "α." The locations of $\alpha_{\rm peak}$ coincide with the known flux rope axis locations (to within the size of the locations marked with "α"). [*See the electronic edition of the Journal for a color version of this figure.*]

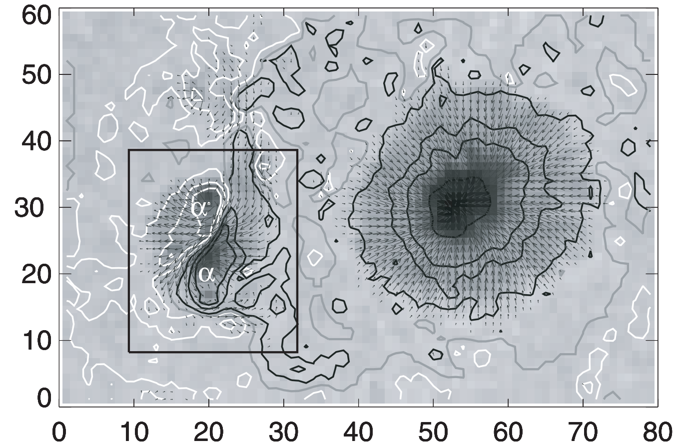

FIG. 4.—Continuum image of NOAA AR 7201 observed 1992 June 19 with the NSO/HAO Advanced Stokes Polarimeter. Contours and arrows are as in Fig. 1. Tick marks are approximately in Mm. The black box outlines the subarea used for consideration of the emerging δ-region only; points marked with "α" indicate the locations of $\alpha_{\rm peak}$. [*See the electronic edition of the Journal for a color version of this figure.*]

helicity at time step 45, as calculated in Fan & Gibson (2004) by the volume integral of the field and vector potential; the agreement is not unexpected since there is yet little if any writhe at this time step. Thus, for this time step, if the α_z at the flux rope axis, i.e., $\alpha_{\rm peak}$, is used, and constant winding rate is assumed, the twist is estimated well.

With the acknowledgment that time step 45 is a bit special (almost fully emerged with coincident peak B_z,α, but with no writhe), we test the significantly earlier time step 30 with this method. The axis location is known, described by the numerical model; it coincides closest now to $\alpha_{\rm peak}$ and is displaced from both the peak B_z (Fig. 3) and $|\boldsymbol{B}|$ locations (not shown, but located slightly offset from the peak B_z and from the known axis location). We find that $\alpha_{\rm peak} = -18.2L^{-1}$ at two locations $d = 0.46L$ apart; the resulting $T/2\pi = 1.04$ (from eq. [1]). The true length of the axis is roughly 50% less than l derived from the semicircle approach, and correcting for that yields $T/2\pi = 0.69$, a very close estimate of the total winding for those field lines near the emerged axis (see Table 1). This estimate of the magnetic wind differs from $H/\Phi^2 = 0.5$ at time step 30 (see Fig. 3 of Fan & Gibson 2004) because the latter is measured for the emerged flux rope as a whole, and at this time step some of the outer winding field lines have not emerged, and their winds are truncated by the lower boundary.

The exercise using time step 30 also illustrates the uncertainty in estimating the twist due to the uncertainty in estimating the axis field-line length. Indeed a lower bound of $l = d$ could be used, and a lower bound of twist could be estimated. There is little to limit the upper bound, and as such, a semicircle is appropriate. If the axis field line is longer due to significant writhe, we take the position that some kinking has already occurred. The $\alpha_{\rm peak}$ approach is thus most appropriate for small, coherent flux ropes and their magnetically connected footpoints rather than the large-scale writhed coronal sigmoid structures.

Thus, to the extent that the axis field-line length can be determined and the assumption of a uniform wind rate is valid (not strictly true for the flux rope), we demonstrate that $\alpha_{\rm peak}$ can recover the wind of the relevant field lines and thus be used to evaluate the fields' susceptibility to the kink instability.

5. DEMONSTRATIONS USING OBSERVATIONAL DATA

NOAA AR 7201 (1992 June) has been extensively studied in the context of the emergence of a small nonpotential δ-spot and the region's subsequent eruption (Lites et al. 1995). The magnetic data, from the National Solar Observatory (NSO)/High Altitude Observatory (HAO) Advanced Stokes Polarimeter (Elmore et al. 1992; Skumanich et al. 1997), are of high spatial resolution and very low noise. When observed on 1992 June 19 (Fig. 4), the active region consisted of a large leading sunspot, a plage area to the northeast, and a small emerging flux region, the δ-spot. Images from the chromosphere and corona (Lites et al. 1995) show a variety of shapes and structures, including neutral-line filaments and large-scale coronal loops with substantial writhe. This region was not observed to erupt by kinking specifically; nonetheless it did produce a number of small flares (Lites et al. 1995; National Geophysical Data Center 2004).

The photospheric vector magnetogram of NOAA AR 7201 as a whole (Table 2) produced $\alpha_{\rm best} = -0.01 \pm 0.03$ Mm^{-1}, indistinguishable from a potential, or untwisted, configuration. The brightest coronal structures presented in Lites et al. (1995) are consistent with the general active region scale, and as such, a rough distance of $d = 40$ Mm is assigned; this implies a representative loop length $l = 63$ Mm. The latter quantity is not important, since given the uncertainty in $\alpha_{\rm best}$, the inferred twist following equation (1) could be $T/2\pi = 0$, implying no twist, or as high as $T/2\pi = 0.37$, consistent with the largest value found in the Leamon et al. (2003) database.

Isolating the emerging δ-spot region (Fig. 4, *boxed area*) gives $\alpha_{\rm best} = -0.28 \pm 0.03$ Mm^{-1}, more than an order of magnitude larger; this is not unexpected, as demonstrated above and

TABLE 2
MEASURES OF TOTAL TWIST IN AR 7201 (1992 JUNE 19)

Object	α (Mm^{-1})	d (Mm)	l (Mm)	$T/2\pi$
	$\alpha_{\rm best}$ Method			
Active region	-0.01 ± 0.03	40	62.8[a]	0.11 ± 0.26
δ-spot.................	-0.28 ± 0.03	10.2	16.02[a]	0.36 ± 0.04
	$\alpha_{\rm peak}$ Method			
δ-spot.................	-0.72 ± 0.3	10.5 ± 0.5	16.5 ± 0.78[a]	0.94 ± 0.41

[a] Assuming $l = \pi d/2$, i.e., a semicircle.

in Leka 1999 and acknowledged in Leamon et al. (2003). The flux-weighted polarity centers give $d \approx 10$ Mm, or a semicircle length $l = 16$ Mm (Table 2). Combining this and again assuming $\alpha_{\rm best} = 2q$ gives $T/2\pi \approx 0.36$, or about a third of the $T/2\pi = 1.0$ considered "baseline" critical. But is there more?

The δ-spot in NOAA AR 7201 strongly resembles the time step 30 magnetogram. Applying the $\alpha_{\rm peak}$ approach we find that $\alpha_z = J_z/B_z$ (box-car smoothed to effectively 2″) peaks in two small regions, one near each flux center, which average to $\alpha_z = -0.72 \pm 0.30$ Mm^{-1}. Both peaks are slightly off of the locations of peak B_z and away from the magnetic neutral line (Fig. 4). These $\alpha_{\rm peak}$ locations are approximately 10.5 ± 0.5 Mm apart, which, assuming constant winding as above and a semicircular axis length, implies $\mathrm{Tw}/\Phi^2 = T/2\pi = 0.94 \pm 0.41$ (see Table 2). Notwithstanding the uncertainties in $\alpha_{\rm peak}$ and the axis field-line length, the unknown amount of writhe in the δ-region's fields, its rapid evolution (Lites et al. 1995), its flare history, etc., the twist portion of the magnetic helicity as estimated here approaches "critical" and could be an *order of magnitude larger* than results using $\alpha_{\rm best}$.

6. CONCLUSIONS

In this study, we perform a "blind test" of a method commonly used to infer twist in active region magnetic fields. The parameter $\alpha_{\rm best}$ is calculated for data arising from a numerical simulation of a helicity-carrying flux tube that emerges into an overlying potential-field arcade, and in which the kink instability criterion is breached. The results from the simulations' "magnetograms" are complemented by a parallel analysis of observational photospheric vector magnetic field data of the well-studied NOAA AR 7201 obtained during the emergence of a δ-spot.

We wish to illustrate two crucial facts. First, while it is well known that portions of solar active regions routinely contain significant magnetic twist, $\alpha_{\rm best}$ calculated for an entire active region fails to detect highly twisted areas. This is noted by Leamon et al. (2003). But even when a highly twisted area is isolated, $\alpha_{\rm best}$ is strongly influenced by the distribution of horizontal fields. This is clear from the test of applying $\alpha_{\rm best}$ to the simulation data, which fails to reproduce the "known" situation. Further, we reiterate through demonstration that $\alpha_{\rm best} = 2q$ is an assumption only valid for a *thin* flux rope, which is not applicable for an active region. If α_z varies, i.e., even if the tube is uniformly winding but not necessarily thin (as with the flux rope in the simulation data), then the simple ratio between α_z and winding rate q only holds at the flux rope's axis, and inferring the wind rate from $\alpha_{\rm best}$ will underestimate the former. Therefore we propose that inferring the vulnerability of entire solar active regions to the kink instability by measuring twist with a method based on the thin flux tube approximation provides at best a lower limit.

But the lower limit of what? The second fact is that in a forced region, when $\boldsymbol{J} \times \boldsymbol{B} \neq 0$, the twist inferred from J_z/B_z may have little relation to the total magnetic twist carried by the magnetic field. If, on the other hand, the vector field is measured in a force-free boundary, localized measures of α_z will reflect the localized total magnetic twist. While it is still the case that $\alpha_{\rm best}$ will underestimate the magnetic twist in anything but a thin flux tube, the results can at least be interpreted directly as a force-free twist.

We propose that by using a slightly different set of assumptions and a measure of α_z derived as an appropriate peak of J_z/B_z near associated footpoints, one may better recover the twist component of the magnetic helicity and thus derive a better estimate of the relevant total twist. This "$\alpha_{\rm peak}$" approach is demonstrated to recover the input to the numerical simulation data at two time steps with different magnetic morphologies. When the $\alpha_{\rm peak}$ approach is applied to the δ-spot of NOAA AR 7201 we find that $T/2\pi$ approaches unity: at least triple the implied total twist derived from the $\alpha_{\rm best}$ approach and possibly indicative of fields susceptible to the kink instability.

The argument concerning event-trigger mechanisms must be refocused to the question of whether large-scale magnetic averages and their inferred connection to large-scale coronal fields are, in fact, the relevant quantities to study. It may be that the detection of small, kink-susceptible areas is most appropriate. We do not argue that the kink instability is the cause of all solar eruptions, but we do argue that many active regions probably carry magnetic twist beyond unity winding number (see Régnier & Amari [2004] for evidence of a highly twisted flux rope with $T/2\pi > 1$ from a nonlinear force-free extrapolation of photospheric vector magnetogram data). A study of "$\alpha_{\rm peak}$" in various active regions, ideally with chromospheric vector field data, is the logical next step. In the meantime, we contend that the kink instability is, in fact, a possible trigger mechanism for solar energetic events and CMEs.

The authors thank Bruce Lites and the helpful referees for their comments on this manuscript. This work was funded by contracts F49620-02-C-0191 and F49620-03-C-0019 with the Air Force Office of Scientific Research. The National Center for Atmospheric Research is sponsored by the National Science Foundation.

REFERENCES

Baty, H. 2001, A&A, 367, 321
Baty, H., Einaudi, G., Lionello, R., & Velli, M. 1998, A&A, 333, 313
Canfield, R. C., Hudson, H. S., & McKenzie, D. E. 1999, Geophys. Res. Lett., 26, 627
Elmore, D. F., et al. 1992, Proc. SPIE, 1746, 22
Falconer, D. A., Moore, R. L., & Gary, G. A. 2002, ApJ, 569, 1016
Fan, Y., & Gibson, S. E. 2003, ApJ, 589, L105
———. 2004, ApJ, 609, 1123
Gold, T., & Hoyle, F. 1960, MNRAS, 120, 89
Hood, A. W., & Priest, E. R. 1979, Sol. Phys., 64, 303
Leamon, R. J., Canfield, R. C., Blehm, Z., & Pevtsov, A. A. 2003, ApJ, 596, L255
Leamon, R. J., Canfield, R. C., Jones, S. L., Lambkin, K., Lundberg, B. J., & Pevtsov, A. A. 2004, J. Geophys. Res., 109, 5106
Leka, K. D. 1999, Sol. Phys., 188, 21
Leka, K. D., & Barnes, G. 2003, ApJ, 595, 1296
Leka, K. D., & Skumanich, A. 1999, Sol. Phys., 188, 3
Lionello, R., Velli, M., Einaudi, G., & Mikić, Z. 1998, ApJ, 494, 840
Lites, B. W., Low, B. C., Martínez Pillet, V., Seagraves, P., Skumanich, A., Frank, Z. A., Shine, R. A., & Tsuneta, S. 1995, ApJ, 446, 877
Longcope, D., & Klapper, I. 1997, ApJ, 488, 443
Longcope, D. W., Fisher, G. H., & Pevtsov, A. A. 1998, ApJ, 507, 417
Moffatt, H. K., & Ricca, R. L. 1992, Proc. R. Soc. London A, 439, 411
National Geophysical Data Center. 2004, Solar Hα Flare Events, http://www.ngdc.noaa.gov
Pevtsov, A. A., Canfield, R. C., & Metcalf, T. R. 1994, ApJ, 425, L117
———. 1995, ApJ, 440, L109
Priest, E. R. 1987, Solar Magnetohydrodynamics (Dordrecht: Reidel)
Régnier, S., & Amari, T. 2004, A&A, 425, 345
Skumanich, A., Lites, B., Martínez Pillet, V., & Seagraves, P. 1997, ApJS, 110, 357
Török, T., Kliem, B., & Titov, V. S. 2004, A&A, 413, L27